5 Tremor Polarization: The Medium

The polarization pattern of Lascar's harmonic tremor described in Section 3.4 is puzzling when viewed in terms of analysis procedures from earthquake seismology. Although each spectral peak has a predominant polarization direction at each station, the wavefield can not be explained as either P, S or surface waves from a single point source. There are three possible explanations. The source radiation may be much more complex than that expected from a point source, giving rise to the polarization patterns observed in Section 3.4. A second possibility is that the source radiation pattern is relatively simple and the path along which harmonic tremor oscillations propagate and the conditions at the measurement site affect the polarization of the measured signals. Finally, at Lascar the particle motion may be produced by some combination from these two contributions. In the first case, the polarization of harmonic tremor can give new insights into the tremor source. If either of the other two possibilities is true, the tremor polarization cannot be used to learn about the source.

Using harmonic tremor recordings from the Lascar network, it is not possible to distinguish between these three explanations. If simple models for propagation effects can produce the observed polarization characteristics, then they may not be used for source modelling without additional evidence. Three simple models for the interaction of harmonic tremor waves with the medium demonstrate possible effects on the polarization: point scatterers in an acoustic medium, the superposition of P and S waves and the effects of reflections at the surface.

5.1 Scattering

The codas of volcanic shocks are an indication that scattering is an important phenomenon in wave propagation in volcanoes [Section 2.3.1, AKI and CHOUET, 1975]. The harmonic tremor wavefield must also be affected. A simple, three-dimensional model of an acoustic medium with no attenuation can demonstrate the qualitative effects of scattering on impulsive wavelets, as well as on continuous sine and square waves.

In the model, a 16 km by 16 km by 16 km grid of scatterers is embedded in an infinite, acoustic medium. Since the medium is infinite, there are no reflections from its boundaries. Because the medium is acoustic, it transmits only compressional waves. Although the volcanic medium is probably highly attenuating, this simple model does not include intrinsic attenuation.

The scatterers are located at randomly selected nodes of the 4096 km^3 grid and their density can be varied. This model uses the Born approximation, which assumes that the scatterers are much smaller than the wavelength of the incident waves.

The velocity amplitude of a spherically propagating, acoustic wave of frequency $\omega = 2\pi f$ from a point source, in a medium in which the velocity of sound is c, is given by INGARD [1988]:

$$\dot{u}(r) = \frac{U_0 a_0}{r} \frac{1 + i/kr}{1 + i/ka_0} \exp(ikr - ika_0) \qquad (5.1)$$

In this equation, U_0 is the velocity amplitude as a function of time at the source-medium interface at radius a_0, while $k=\omega/c$ is the wave number. The wave propagating a distance r from an isotropically scattering monopole, s, at r_s takes on the same form,

$$\dot{u}_s(r) = \frac{\dot{u}(r_s) a_s}{r} \varepsilon_s \frac{1 + i/kr}{1 + i/ka_s} \exp(ikr - ika_s) \qquad (5.2)$$

with the exception that U_0 is replaced by $\dot{u}(r_s)$, the amplitude of the incident wave at the location of the scatterer, times the scatterer's efficiency, ε_s, and a_0 is replaced by the diameter of the scatterer a_s. For small values of ka_s, that is when the wavelength is much larger than the radius of the scatterer (Born approximation), the scatterer's efficiency is

$$\varepsilon_s = \sqrt{\frac{\theta_s}{[(\theta + \theta_s)^2 + (\chi + \chi_s)^2]}}\,. \qquad (5.3)$$

θ and θ_s are the normalized radiation resistance of the medium and the scatterers, while χ and χ_s are their respective reactances. This number can never be greater than 1, and varies depending on the characteristics of the medium and scatterers [INGARD, 1988]. In the model, each scatterer is randomly assigned a scattering efficiency, $0 < \varepsilon_s < 1$. This very simple

model holds when the density of scatterers is low, so that the incident wave at any point in the model can be assumed not to have lost any energy to scattering. If the scatterers are more dense, the incident wave at the scatterer will have lost energy and have a lower amplitude than that given in Equation 5.1. If the direct wave has travelled a distance r, the loss as compared to the wave amplitude with no scattering can be estimated as [INGARD, 1988]:

$$C_{scat} = \exp\left(-\frac{r < \varepsilon^2 > \sigma_{scat} \rho_{scat}}{2} \right) \tag{5.4}$$

where $<\varepsilon^2>$ is the root mean square scattering efficiency, $\sigma_{scat} = 4\pi a_s^2$ is the scatterer cross-section and ρ_{scat}, the density of the scatterers, is taken to be the inverse of the cube of the mean interscatterer distance, δ_{scat}. For this model, I take both a_0 and a_s to be 100 m, half the separation of the grid points, and the velocity of sound to be c = 1000 m/s. Strictly speaking, the Born approximation implies that for this geometry, the model is only valid for frequencies below 3 Hz.

Figure 5.1 shows the geometry of one plane of the scattering medium containing the source (X) and receiver (O) for a realization of a densely scattering medium. The seismogram at the receiver location is the sum of contributions from the source and from the single scattering contribution of each point of the scattering grid.

$$\dot{u}_r = C_{scat}(r_0)\dot{u}(r_0) + \sum_s C_{scat}(r_s)\dot{u}_s(r_{s0}) \tag{5.5}$$

For each node the incident amplitude is corrected for attenuation due to scattering using Equation 5.4.

If the source only radiates at a single frequency, i.e. a sine wave, it is easy to use this equation to calculate its outwardly propagating wave and the corresponding scattered waves in the time domain and superpose them at the location of the receiver to generate the expected seismogram for the configuration of scatters. If the source has a finite bandwidth, however, the problem becomes more difficult because of the frequency dependent product

$kr = \omega r / c$ in Equations 5.1 and 5.2. I have therefore calculated the theoretical seismograms discussed in the following paragraphs in the frequency domain. First, the source seismogram is Fourier transformed. For each scatterer, s, this spectrum is multiplied by the amplitude factor describing the geometric distance decay and that due to scattering losses and by the phase factors describing the phase shifts due to the distance traveled to the scatterer s. The spectrum is further multiplied by geometric distance decay factors and phase shifts for the distance between the scatterer and the receiver. The resulting spectrum for the contribution to the seismogram from the scatterer s is resolved into a radial component, parallel to the direction between the source and the receiver, and a transverse component perpendicular to it in a chosen plane. Since these calculations are made under the assumption of acoustic scattering, the radial and transverse components at the receiver location depend only on the direction between the scatter and the receiver. The radial and transverse contributions for each scatterer in the scattering model are added to the radial and transverse receiver spectra of the direct wave before they are inverse Fourier transformed to give the synthetic

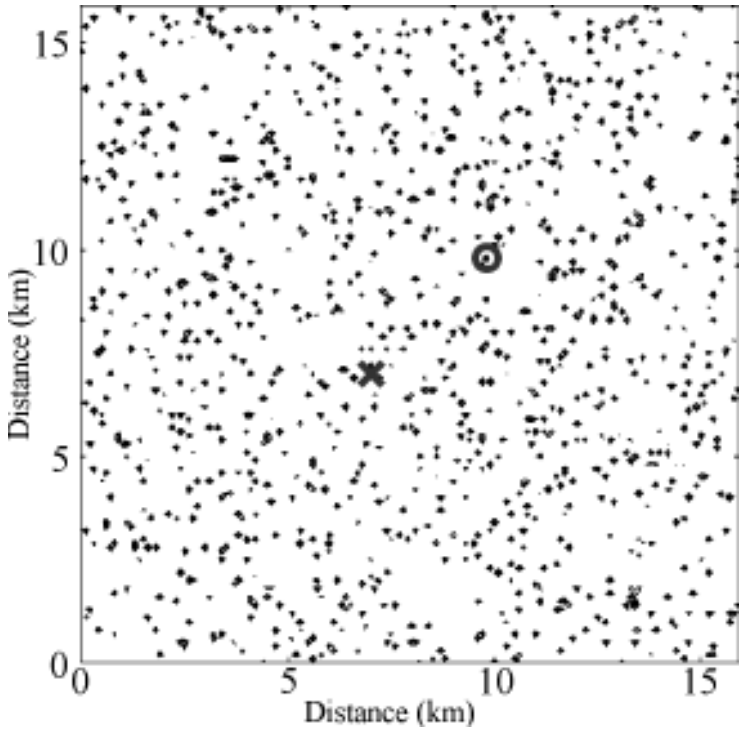

Figure 5.1 One plane of the three-dimensional sample scattering space containing the source (X) and receiver locations (O). The mean scatterer separation in three dimensions is 0.45 km. The distance between the source and receiver is 3.96 km.

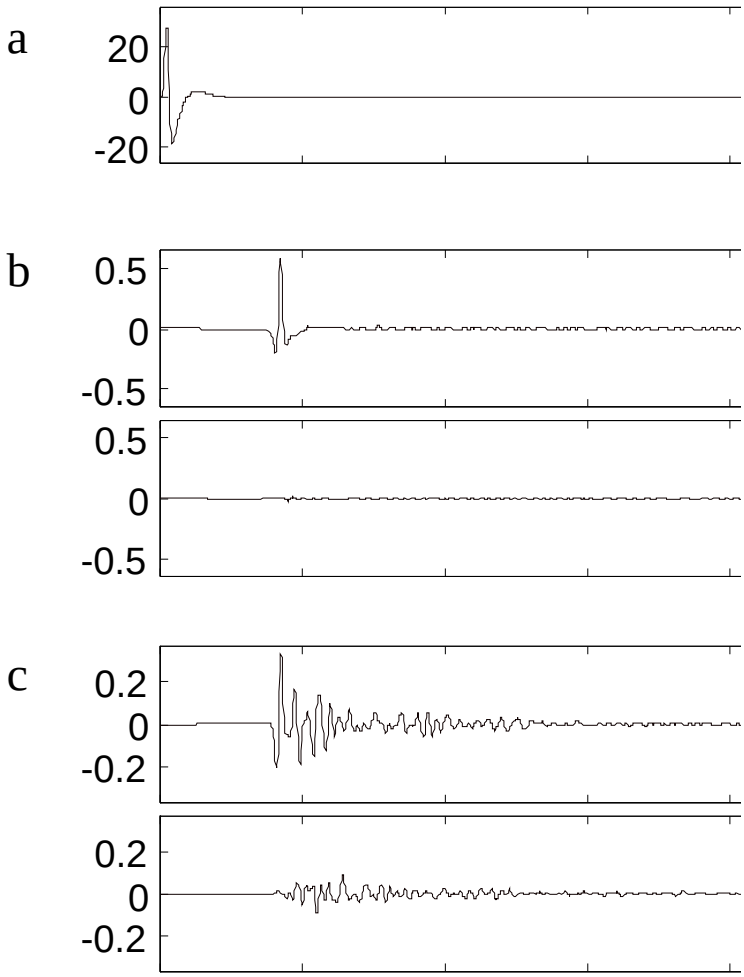

Figure 5.2 Source and scattered seismograms for an impulsive source. (a) The seismogram of ground velocity at the source. (b) Radial and transverse seismograms are plotted for a very sparse system of scatterers, 495 scatterers in 4096 km^3 and δ_{scat} = 2.0 km. (c) and (d) Seismograms for more densely scattering media with 25246 scatterers and δ_{scat} = 0.55 km and 50509 scatterers and δ_{scat} = 0.43 km, respectively.

seismograms. The only disadvantage of this method is the acausality introduced by the manipulation of the spectra. It is apparent as a low level of energy that arrives at the receiver before the arrival of the direct wave.

If there are no scatterers, the wavefield at the receiver is by assumption only radial, regardless of the duration and shape of the source function. With scatterers, the situation changes. For an impulsive source, like an earthquake or explosion, these effects are familiar to analysts as the coda (Figure 5.2). The amplitude of the source for this and later figures is normalized so that the product of source amplitude and source radius are approximately equal to the amplitude of the incident wave excluding attenuation due to scattering times the source-receiver distance, $U_0 a_0 = \dot{u}(r_0) r_0$. Far from being narrowband, the spectrum of the impulsive source is broadband with contributions from many wavenumbers k=ω/c. The effect of a medium with low scattering density is small, producing a small coda and a low level of energy on the transverse component (Figure 5.2b). The coda is effectively a transient which continues from the time of the first arrival until waves reflected from the most distant scatterers have returned to the receiver location. After the incident wave has passed the most distant scatterers, no more energy returns to the receiver, and the coda ends. When the number of scatterers increases, the simple, impulsive source function produces a seismogram similar to those measured for volcanic shocks like rapid fire tremor (Section 2.3.1), volcano-tectonic events and earthquakes. The energy is partitioned between the radial and transverse components (Figure 5.2c). The amplitude of the coda on the transverse component depends on the location and strength of the scatterers. When the density of scatterers is high, the maximum amplitude of the synthetic seismogram may be shifted from the onset to later in the seismogram, as it is in Figure 5.2d.

Unlike shocks which have an impulsive source, tremor signals continue for long intervals. A very simple example of such signals are tremor which have the appearence of a sine wave. These are narrowband signals which begin at some time, t = 0 s, and then continue on indefinitely (Figure 5.3a). If the density of scatterers is low (Figure 5.3b), the wavefield at the receiver site is similar to that in a medium without scatterers. The seismograms are nearly radially polarized. After the first arrival, the wave appears to continue unchanged until

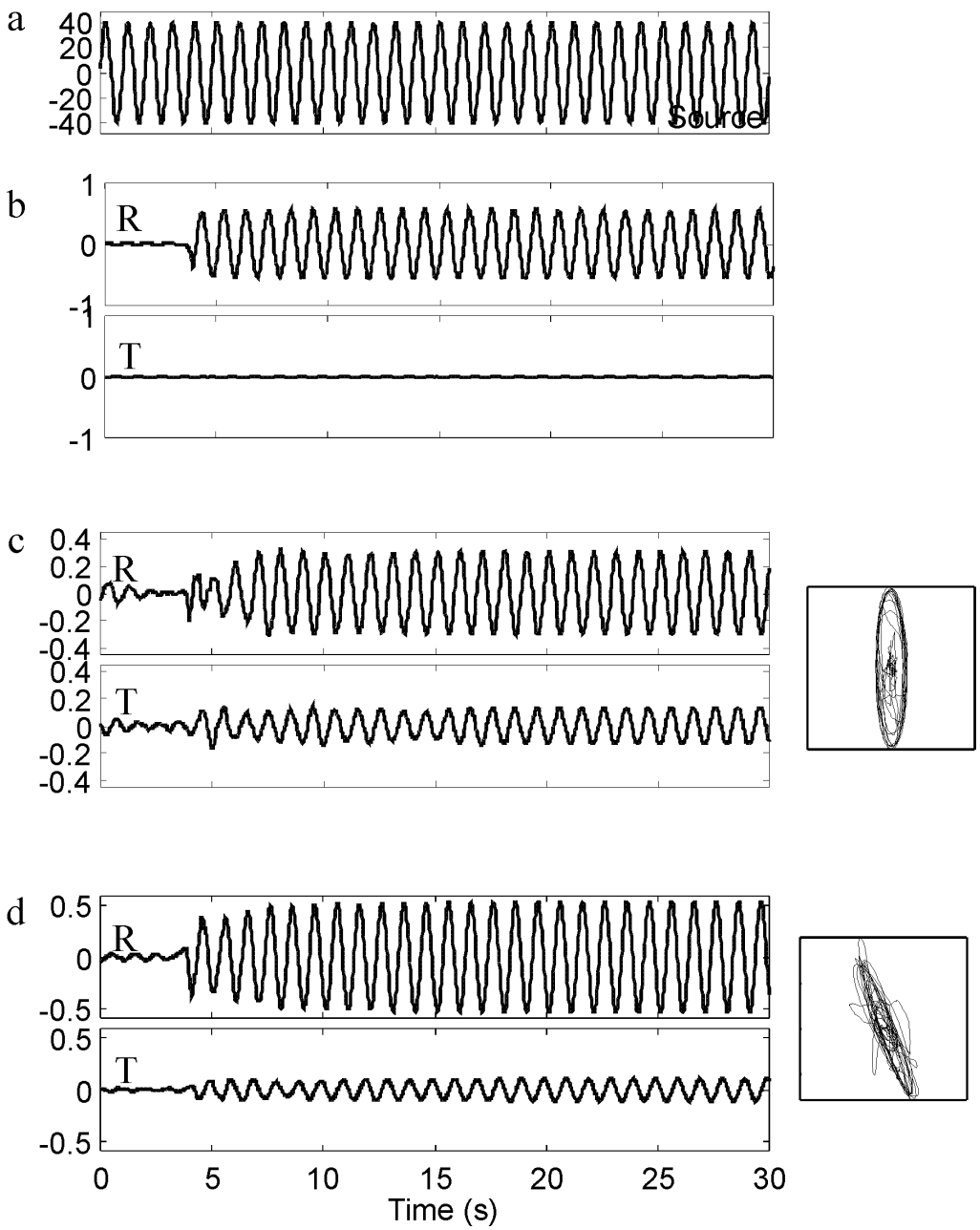

Figure 5.3 Source and scattered seismograms for a source generating a sinusoidal wavefield (1.0 Hz). (a) The seismogram of ground velocity at the source. (b) Radial and transverse seismograms are plotted for a very sparse system of scatterers, 451 scatterers in 4096 km^3, with δ_{scat} = 2.0 km. (c) Radial and transverse seismograms for a more densely scattering medium with 25246 scatterers and δ_{scat} = 0.55 km along with particle motion in the R-T plane. In this plot and all other particle motion diagrams, the radial axis is vertical and the transverse axis is horizontal. Both axes have the same scale. (d) Radial and transverse seismograms for a medium with 50509 scatterers and δ_{scat} = 0.43 km, along with the particle motion in an R-T plane. After a transient following the first onset (~ 5 s), the particle motion is constant and is not necessarily related to the source-receiver direction.

the end of the interval shown and the amplitude on the transverse component is very low. When there are more scatterers, however, there is a transient after the initial onset (Figure 5.3c). This is the interval between the first arrival and the time in which the outwardly propagating wave reaches the limits of the scattering medium and the scattered waves from the most distant scatterers return to the receiver. As the medium is infinite, there is no reflected wave. During this interval, the amplitudes of both the radial and transverse components change as the effects of more scatterers join the signal. After the transient stops, at about 10 s in this model, the amplitudes of both components remain constant, as does their relative phase. In general, the amplitude and phase of the transverse component depends on the location and strength of the scatterers. If the transverse component is in phase with the radial component (Figure 5.3d), the particle motion at the receiver site will be rotated from the radial and linearly polarized. The angle of rotation depends on the relative amplitudes of the two components. As the phase delay between the two components increases, the rectilinearity decreases. The particle motion no longer necessarily points to the source.

The results for a square wave source provide insights into the effects of propagation on Lascar's harmonic tremor (Figure 5.4). The square wave's spectrum is a sequence of narrowband peaks indicating that its wavefield is made up of waves with discrete wavenumbers $k_n=\omega_n/c$. If there are few scatterers, the transient is so small that it appears to be missing and the waves arriving at the receiver are primarily radially polarized (Figure 5.4b). Because there is little energy on the transverse component, each of the spectral lines is also radially polarized and highly rectilinear. When the number of scatterers increases, the transient after the onset lasts until the medium is saturated with outgoing and scattered radiation. The level of energy on the transverse component also increases. At the same time, for a given scatterer the relative phase for the different peaks depends on the wavenumber, $k_n r$. Thus, when the spectra from the many scatterers are superimposed at the receiver site, the polarization is different for each spectral peak and is not necessarily related to the source-receiver direction (Figures 5.4c and 5.4d). A small change in either the

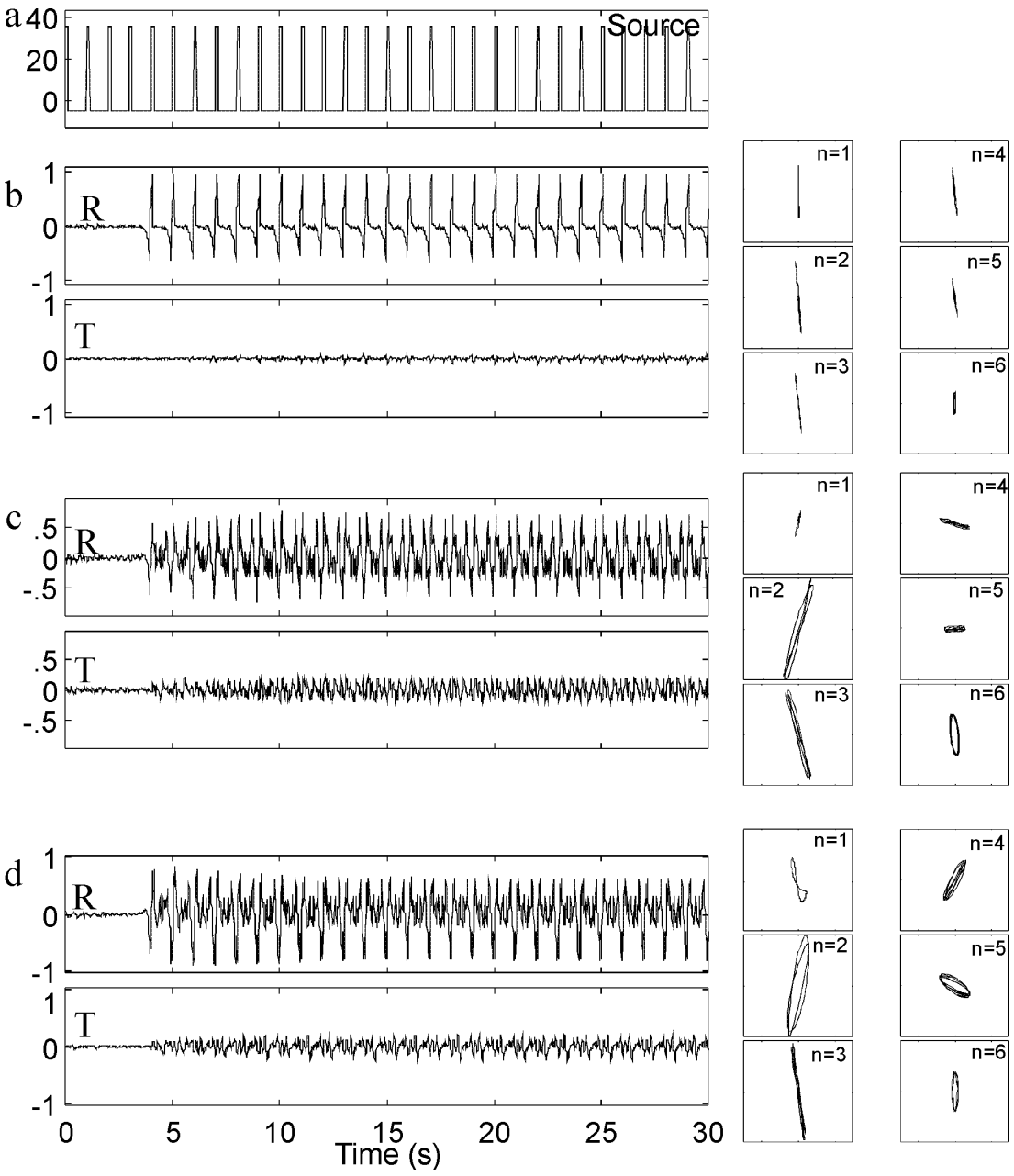

Figure 5.4 Source and scattered seismograms for a 1.0 Hz, 13% square wave source. (a) The seismogram for ground velocity at the source. (b) Radial and transverse seismograms are plotted for a very sparse system of scatterers, 528 scatterers in 4096 km^3 and δ_{scat} = 2.0 km. The particle motion diagrams show the particle motion for the data filtered to extract the first 6 harmonics. (c) and (d) Seismograms and particle motion diagrams for the first six harmonics for more densely scattering media with 24934 scatterers and δ_{scat} = 0.55 km and 50582 scatterers and δ_{scat} = 0.43 km, respectively. The particle motion diagrams (horizontal axis T, vertical axis R) are taken from the interval between 20 s and 30 s, after the end of transient following the first onset. They show the polarization of the energy for the spectral lines $f_n = nf_1$, n=1, 2, 3, 4, 5, 6. For these plots the bandpass filter corner frequencies were [0.5, 1.5] Hz, [1.5, 2.5] Hz, [2.5, 3.5] Hz, [3.5, 4.5] Hz, [4.5, 5.5] Hz and [5.5, 6.5] Hz.

density of scatters or their location can completely change the pattern of particle motion as a function of frequency.

This acoustic model of single scattering with no attenuation demonstrates that even a simple system of scatterers can mimic important characteristics of volcanic shocks and tremor. The strong coda present in the shocks of rapid fire tremor (Figure 2.3a) indicates that scattering is an important process affecting the volcano's wavefield. A quantitative investigation of the volcano's structure using this extremely simple and qualitative scattering model to synthetically emulate the shocks' coda would, however, overrate the validity of the model. The three components of the shock records depend on the more complicated and yet unknown source process, as well as the direct and scattered P, S and surface waves. To properly model the shock codas requires an exhaustive investigation of these variables along with the effects of changes in scatterer size and efficiency and wave velocity.

This scattering model only allows qualitative conclusions about the volcanic medium. It must have many scatterers. Small, arbitrary changes in the locations and strengths of the scatters have a large effect on the polarization. The model also provides an explanation for the apparently unusual behavior of the polarization of the different frequency peaks of harmonic tremor at Lascar Volcano (Section 3.4).

5.2 Superposition

Normally a double couple, impulsive source will generate both P and S waves. Because the P waves, which are compressional waves, travel at a higher velocity than the S waves, they arrive at the station before the S waves which are transversely polarized. Explosive sources only excite P waves, but these may be converted near the source, so that the explosion's wavefield also includes both P and S waves. In the farfield of a single, impulsive source, the two types of waves are well separated in time. If the source is continuous, the recordings at the receiver location will be a superposition of both wavetypes. A very simple, two dimensional experiment can qualitatively demonstrate the effects of the concurrent arrival of these two wavetypes with the same frequency content on the polarization observed at a recorder. The geometry of the model is similar to that of the plane shown in Figure 5.1.

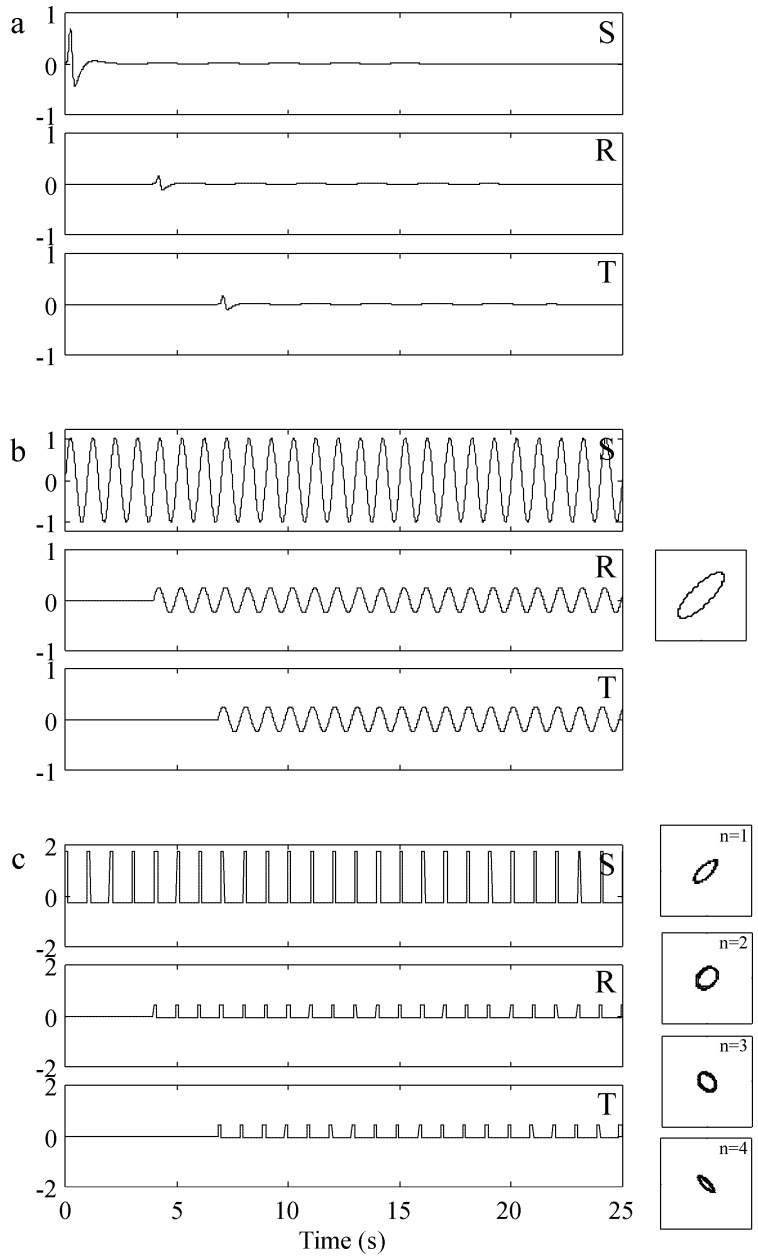

Figure 5.5 Source and station seismograms for a medium with P and S waves. The P-wave and S-wave velocities are α = 1.0 km/s and β = 0.58 km/s. The distance between the source and station is 3.96 km. (a) Seismograms for a source pulse (S) and the radial (R, P wave) and transverse (T, S wave) arrivals at the station. (b) Seismograms for a sine wave source (1 Hz) and the radial and transverse seismograms at the station. The particle motion diagram shows the polarization under steady-state conditions. (c) Seismograms for a 13% square wave source (1 Hz) and the radial and transverse seismograms at the station. The particle motion diagrams show the polarization for the spectral lines $f_n = nf_1$, n=1, 2, 3, 4 under steady-state conditions. For these plots the bandpass filter corner frequencies are [0.5, 1.5] Hz, [1.5, 2.5] Hz, [2.5, 3.5] Hz and [3.5, 4.5] Hz.

The medium, however, has no scatterers and conducts both compressional waves that travel at α = 1000 m/s and transverse waves that travel at $\beta = \alpha/\sqrt{3}$.

In the farfield of a single, impulsive source, the two wavetypes arrive separately (Figure 5.5, top) and the polarization for each arrival is well defined. When the source is continuous, the polarization becomes more complex. For a sine wave (Figure 5.5 middle), the compressional waves arrive first, but because they are generated continuously, they are still present when the first S-waves arrive, with a different phase and on the transverse component. Rather than producing separate movement as with the impulsive source, the particle motion is rotated from the radial or transverse. The polarization angle depends on the phase difference between the two waves, which in turn depends on the wave velocities and the distance travelled.

The model wave for harmonic tremor, a 13% square wave (Figure 5.5, bottom), also produces a superposition of phase-shifted P and S waves. The polarization for each harmonic depends, as it did for the sine wave, on the phase of the contributions from each wavetype. Because the phase-shifts depend on the frequency and the distance travelled, the polarization is different for each spectral peak. For each of the harmonics shown in the particle motion diagrams, the polarization direction bears no apparent relationship to the propagation direction of the seismic waves.

5.3 Surface Reflections

In a homogeneous space, the particle motion of P waves is parallel to the source-receiver direction, while that of S waves is perpendicular to it. The reflections generated by P or S waves at a free surface, such as a seismometer site, have been described by NUTTLI and WHITMORE [1961] and NUTTLI [1961], respectively. The recorded seismogram is a sum of the particle motion due to the incoming wave and the reflected waves.

The case for P waves is fairly simple. At the free surface, an incoming P wave generates a reflected P wave and a reflected S_V wave. All of the motion is in the plane defined by the wave propagation ray and the vertical direction, and the azimuth determined from the particle

motion points toward the source. In contrast, the inclination of the particle motion or apparent incidence angle, $\bar{i}_0$, is distorted from the incidence angle of the incoming ray, i_0:

$$i_0 = \sin^{-1}\sqrt{(1-\cos\bar{i}_0)\alpha^2/\beta^2}\ . \qquad (5.6)$$

If the P and S wave velocities, α and β, are known, the incidence angle of the incoming wave can be calculated from the apparent incidence angle.

S waves produce a more complicated picture. The motion due to the part of the S wave parallel to the Earth's surface, S_H, is reflected simply, producing only a reflected S_H wave. Since the particle motion for this wave is perpendicular to the direction of propagation and parallel to the surface of the earth, the recorded ground motion is

$$\bar{u}_H = 2U_H\cos\omega t \qquad (5.7)$$

if $U_H\cos\omega t$ is the S_H ground motion due to the incoming wave. The particle motion due to the rest of the incident S wave, called S_V, is perpendicular to S_H and to the incidence angle, j_0, at an angle 90-j_0. Like the P wave, all of its energy is in the vertical plane defined by the propagation direction. This wave produces a reflected S_V wave at an outgoing angle j_0 and a reflected P wave at an outgoing angle i_0. There are two more complications to this situation. The particle motion of the incoming and outgoing S_V waves have the same vertical amplitude but opposite horizontal motion. Adding them together gives motion that is only vertical. Also, when the incidence angle of the incoming S_V wave is sufficiently large, $j_0 > \sin(\beta/\alpha)$, then $\sin i_0$ is greater than 1, and i_0 is imaginary [NUTTLI, 1961]. Thus, the particle motion due to S waves recorded at the seismometer depends strongly on the incidence angle of the incoming wave and the ratio of S_H to S_V energy. Figure 5.6 shows the particle motion for incidence angles between 0º and 90º. The particle motion is calculated assuming that $\beta = \alpha/\sqrt{3}$ and that the ground motion due to the incident S_V waves is $U_V = U_H\cos\omega t$, that is, energy is evenly partitioned between S_H and S_V waves and they are in phase. Between 35º and 40º the particle motion becomes non-linearly polarized as the outgoing angle for the reflected P-wave becomes complex. NUTTLI (1961) gives an excellent summary of the expected particle

motion due to S waves under various incidence angles and different ratios of S_H to S_V energy.

If the wavefield consists of S waves in an isotropic medium, then a receiver on the surface will record complex motion due to the incoming S_H and S_V energy and all the concomitant reflected waves. Normally a seismic station is assumed to rest on a horizontal surface and the source to lie below the surface. In fact, most volcano stations, as those at Lascar, are installed on slopes, and the source may lie in the crater at a higher altitude than the station. In such cases the incident angles may easily exceed $\sin^{-1}(\beta/a)$.

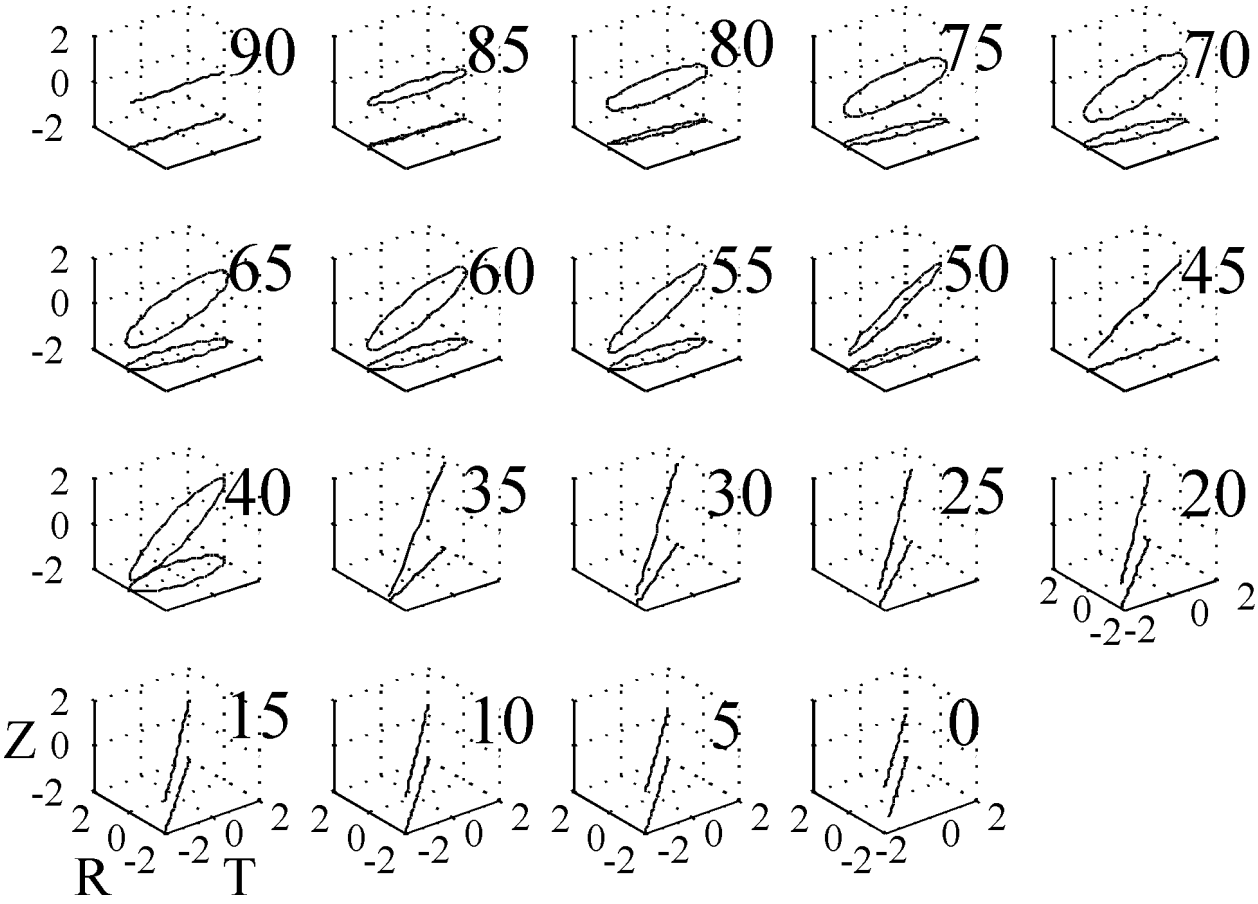

Figure 5.6 Particle motion for S waves (S_H/S_V ratio = 1) reflected at a horizontal surface in an isotropic medium for various incidence angles. The particle motion is given in the coordinate system [transverse (T) - radial (R) - vertical (Z)]. The incidence angle is measured from vertically down.

5.4 Summary

It is inviting to use the particle motion of a propagating wave, as in earthquake analysis, to learn more about the source, either by drawing conclusions about its location or the types of waves it is generating. Unfortunately, the polarization of the different spectral peaks of Lascar's harmonic tremor described in Section 3.4 cannot be used in this fashion. The particle motion may be caused either by source complexity, by propagation effects, or by some combination of these two factors.

The simple models for propagation effects presented in this chapter indicate that the observed polarization characteristics can be produced in continuous signals by path and site conditions. Taken individually each model reproduces some of the polarization and phase characteristics observed in harmonic tremor. Realistically, factors from all three models must in some way be represented in the Lascar. Scattering is certainly an important factor in wave transmission, as are the presence of P and S waves and their reflections at the surface. Even if Lascar's harmonic tremor began at the source with a simple polarization and with a well-defined phase relationship between the overtones, after passing through even a simple volcanic medium which could be described by these models, the polarization and waveforms would be very complex. Any source complexities affecting the polarization and phase of the harmonics are completely masked by these effects.

6 Conclusions

Like other active volcanoes, Lascar generates many different kinds of seismic signals. The interval of harmonic tremor, with its regularly peaked spectrum, recorded by PISCO's Lascar network is unique in its number of overtones and its duration. Similar signals observed at other volcanoes only occur during a short interval following a triggering event and have only a few overtones [Kamo et al., 1977, Mori et al., 1989, Schlindwein et al., 1995, Benoit and McNutt, 1997, Hagerty et al., 1997, Lees et al, 1997].

Even at Lascar, episodes of harmonic tremor are relatively rare. Nonetheless this type of tremor provides new insights into the inner workings of volcanoes. Because it so obviously does not fit the accepted source models for volcanic tremor [for example, Chouet, 1996, Schlindwein et al., 1995, McNutt, 1994], it also demands their reexamination and invites the proposal of new models. On further evaluation these new models may be seen to apply not only to the special case of harmonic tremor, but more universally to other types of tremor.

The standard methods for seismological data analysis were developed for the investigation of events, broadband wavelets with a distinct beginning and with a definable end. In contrast, volcanic tremor is a continuous signal generated by a persistent process. It usually has neither a clear beginning nor end. Often, it also has narrow band peaks in its spectrum. Common methods of seismological data analysis can provide a foundation on which to base tremor analysis. However, they miss much of the information encoded in the wavefield. The new methods presented here for analyzing the tremor frequencies as a function of time and for analyzing polarization offer additional insights into the behavior and characteristics of volcanic, and in particular harmonic, tremor.

The polarization of the wavefield of a impulsive source, measured using three component recordings from several stations, can often provide information about the location of the source or the type of wave. Unlike the polarization of first arrivals from events, however, the polarization of the harmonic peaks seems to be unrelated to the direction to the active crater, their probable source. Indeed, the particle motion of any given peak cannot be explained as a simple wavefield of P, S or surface waves from a single source. It is possible that the observed polarization patterns are caused by a complex and extended source.

However, they can also be explained as propagation effects on a steady-state wavefield. Scattering, the superposition of P and S waves and surface reflections affect the polarization of continuous waves in ways that mimic the recordings of harmonic tremor at Lascar. Before the particle motion can be used to derive source characteristics, such effects must be excluded. On the otherhand the long term stability of harmonic tremor's polarization indicates that the source remains in the same place for extended intervals.

The most striking feature of harmonic tremor is its cyclic nature. In the seismograms, the waveforms are highly repetitive, changing only slowly over the course of many periods. In spectra, the cycles take the form of a regular series of extremely sharp peaks which can be characterized by $f_n(t) = nf_1(t)$, where $T = 1/f_1(t)$ is the period of the cycles. The peaks are observed at the same frequencies at all the Lascar stations, indicating that they are a characteristic of the process generating the harmonic tremor.

Many models have been proposed for the source of volcanic tremor (Seidl et al, 1981, Ferrick *et al*, 1982, Julian, 1994). Several attempt to explain tremor characterized by narrow spectral peaks as the oscillatory response of a gas or fluid-filled body to some unspecified force (Mori et al, 1989, Schlindwein et al, 1995, Chouet, 1996). These models have two disadvantages. First, while the authors relate the frequencies of the peaks to geometric parameters which are volcano specific, many volcanoes throughout the world have peaks at similar frequencies. Thus, the tremor source must have characteristics that are not volcano dependent and that can vary over short (30 s) intervals by 30% or more (Benoit and McNutt, 1997, Hellweg, 1997, Lees et al, 1997, Hagerty et al, 1996). Second, with these models their proponents describe a static picture of the volcano, neglecting the forces and processes which are necessary to excite the oscillations. The harmonic tremor of Lascar, along with the high quality of the recordings and the insights from the methods presented here provide an improved foundation for new, physical models for the source.

Here, I present the three new models for the source of harmonic tremor which relate the tremor to dynamic flow processes in the volcano. The models are based on the results of both standard and new analysis methods. For the three models, eddy shedding, slug flow and soda bottle, the observed characteristics of the tremor, in particular its fundamental

frequency and the shape of the power spectrum are related to fluid dynamic variables of the models such as characteristic flow dimension (i.e. conduit size), kinematic viscosity of the fluid and flow velocity. Estimates of the signal amplitude generated by the eddy shedding and slug flow models suggest that the moving fluid is probably water.

All three models give the same result: If the flow dimensions and velocities are to remain within reasonable bounds,

1. Harmonic tremor must be generated by the **movement of water or gases like steam**, not magma,
2. Harmonic tremor must be generated **near the surface,** close to atmospheric pressure, therefore probably in the active crater, and
3. Changes in the tremor frequency are caused by **small, easily reversible changes in flow velocity**, rather than by changes in the geometry of the volcano's conduit system.

In addition, the physical processes described by the models occur in specific ranges of flow "amplitude" as described by the Reynolds number. If the Reynolds number is lower or higher, as it would be during other flow regimes, the same flow geometery would generate other types of signals. The sound associated with turbulent flow systems, for example, is considered broadband noise (MORSE and INGARD, 1968, TRITTON, 1988, FABER, 1995). Thus, these models may be applicable at many volcanoes and may, in addition, explain the continuous "background" tremor as part of the same phenomenon. If these models are correct, harmonic tremor, and perhaps other forms of tremor, are symptoms of activity in the hydrothermal system of the volcano. Increases in tremor amplitude may then be related to increases in heat flow.

Although each volcano is unique, many share a characteristic: the tremor at many volcanoes has one or more sharp peaks between 0.5 and 2 Hz. One important question of volcano seismology has been to find the uniting factor which will explain such similarities. The models for harmonic tremor presented here provide the common factor: harmonic tremor is generated by the flow of heated gases or water in the near-surface hydro/gas-thermal system of the volcano.